JOURNAL OF GEOPHYSICAL RESEARCH, VOL. 102, NO. D25, PAGES 29,901–29,915, DECEMBER 27, 1997

Atmospheric absorption during the Atmospheric Radiation Measurement (ARM) Enhanced Shortwave Experiment (ARESE)

Charles S. Zender,[1] Brett Bush,[2] Shelly K. Pope,[2] Anthony Bucholtz,[2]
William D. Collins,[1,2] Jeffrey T. Kiehl,[1] Francisco P. J. Valero,[2]
and John Vitko Jr.[3]

Abstract. The objectives of the Atmospheric Radiation Measurement (ARM) Enhanced Shortwave Experiment (ARESE) are to directly measure clear and cloudy sky shortwave atmospheric absorption and to quantify any absorption found in excess of model predictions. We undertake detailed model comparisons to near-infrared and total solar flux time series observed by surface and airborne radiometric instruments during the ARESE campaign. Model clear-sky absorption biases generally fall within the range of uncertainty generated by sample size, and assumptions of aerosol properties and surface albedo. Direct measurements by stacked aircraft on the overcast day of October 30, 1995, confirm the detection of enhanced cloud shortwave absorption during ARESE. The detection is substantiated by, and consistent with, three independent measures of cloudy sky absorption estimated in previous studies: cloud forcing ratio, insolation forcing ratio, and albedo/transmission slope. A significant portion of the enhanced absorption occurs at visible wavelengths. Collocated measurements of liquid water path (LWP) suggest the magnitude of the enhanced absorption increases with LWP.

1. Introduction

The most fundamental quantity determining Earth's climate is the amount of solar radiation absorbed by the climate system. This flux of energy is determined by the amount of shortwave radiation both reflected and absorbed by the system. Over the years, satellite data have constrained the first of these quantities, that is, the reflectance of the planet. It is only in the past few years that attempts have been made to determine the amount of shortwave absorption in Earth's atmosphere. Presently, this is one of the least quantified properties of the climate system [*Kiehl and Trenberth*, 1997]. A major component in determining the disposition of shortwave radiation in the atmosphere is the presence of clouds.

Radiation models indicate that cloudy skies absorb about as much shortwave energy as clear skies. Observations of how much shortwave radiation is absorbed in clouds suggest discrepancies with these models. In particular, observations suggest that clouds may absorb more shortwave radiation than is modeled [*Stephens and Tsay*, 1990]. Recent studies by *Cess et al.* [1995], *Ramanathan et al.* [1995], *Pilewskie and Valero* [1995], and *Waliser et al.* [1996] indicate that clouds absorb considerably more shortwave radiation than current radiative transfer models suggest. Indeed, the amount of cloud absorption found in these more recent studies is much greater than many previous studies suggest. This disparity between observed and modeled cloud absorption has prompted a vigorous debate in the atmospheric radiation community. There have also been suggestions by *Arking* [1996] that any enhanced atmospheric absorption above model predictions occurs in clear-sky regions and not in clouds.

This disparity in interpretation of atmospheric absorption prompted the Atmospheric Radiation Measurement (ARM) program to initiate a field experiment at the Southern Great Plains site in Oklahoma, which was carried out in 1995. The focus of the present study is to present a detailed analysis of data collected during this experiment and to determine if there are indications of enhanced atmospheric absorption above that predicted by current radiative transfer models. Furthermore, the focus is to determine if this enhanced absorption occurs mainly in clear or cloudy sky conditions. Finally, the study investigates whether the findings from the ARM Enhanced Shortwave Experiment (ARESE) support analysis techniques and findings of the studies by *Cess et al.* [1995], *Ramanathan et al.* [1995], and *Pilewskie and Valero* [1995].

This study is organized as follows: section 2 presents a description of the observational data and model employed for the analysis of atmospheric absorption, section 3 presents the results of the analysis in terms of surface insolation, albedo, and column absorption, and section 4 provides a discussion and summary of these results in light of previous studies.

2. Methods

2.1. ARESE Campaign

The ARM Enhanced Shortwave Experiment (ARESE) was conducted at the Department of Energy (DOE) ARM Southern Great Plains (SGP) Central Facility between September 22 and November 1, 1995. The principal objectives of ARESE were (1) to directly measure the absorption of solar radiation

[1]National Center for Atmospheric Research, Boulder, Colorado.
[2]Scripps Institution of Oceanography, University of California at San Diego, La Jolla.
[3]Sandia National Laboratories, Livermore, California.

Paper number 97JD01781.
0148-0227/97/97JD-01781$09.00

by the clear and cloudy atmosphere and to place uncertainty bounds on these measurements; and (2) to investigate the possible causes of absorption in excess of model predictions. The standard radiometric instrumentation at the Central Facility was augmented with the addition of high-precision instruments starting on October 11 [*Valero et al.*, this issue (a)]. Matching instruments were flown on board a twin-engine Otter turboprop, a Grob Egrett, and the NASA ER-2. The Otter was flown at or below the top of the boundary layer in order to measure the visible and near-IR radiation near the Earth's surface. The Egrett was flown in the lower stratosphere in coordinated flight with the Otter. Data from the coordinated flights gives the flux divergence between the two aircraft in a column spanning most of the troposphere. The Otter and Egrett were based at the Blackwell/Tonkwa airport east of the Central Facility and flew along two predetermined flight tracks selected on the basis of prevailing meteorological conditions [*Valero et al.*, this issue (b)]. The flight tracks included overflights of the Central Facility and the boundary facilities at Byron, Coldwater, Vici, and Ringwood. The ER-2 was based near Austin, Texas. It was used to calibrate the GOES satellites against radiometers on the aircraft and to validate estimates of broadband albedo derived from satellite imagers.

The analysis in this paper includes the data from the Central Facility, the Otter, and the Egrett. Eleven coordinated flights were conducted with these aircraft between September 25 and November 1, 1995. Data from October 11 and October 30 are used to study the absorption in clear-sky and cloudy conditions, respectively. Measurements from October 15 are used to compare model and observed clear-sky transmission under conditions of very low aerosol turbidity. The observations on October 13, 17, and 19 are used to study the relation of albedo and transmission (section 3.4.3) under conditions of broken and scattered cloud cover. The data employed in the present study were obtained from the ARM data archive (http://www.archive.arm.gov) and were current as of August 15, 1997. Subsequent minor modifications to the data have not been included.

2.2. Description of Radiometric Instruments

ARESE followed the experimental strategy of coeval radiometric measurements above and below cloud by multiple aircraft as discussed by *Pilewskie and Valero* [1995]. Three aircraft were used for the experiment: the NASA ER-2 high-altitude aircraft flying at about 20 km altitude, a Grob Egrett flying around 14 km, and a Twin Otter flying from 0.5 to 2.0 km. Additionally, three special surface radiometric stations supplemented the regular Cloud and Radiation Testbed (CART) instruments. Each aircraft was equipped with identical sets of zenith and nadir pointing radiometers each consisting of (1) a Total Solar Broadband Radiometer (TSBR) to measure spectral broadband (0.224–3.91 μm) solar irradiance, (2) a Fractional Solar Broadband Radiometer (FSBR) to measure near-infrared (0.68–3.3 μm) solar irradiance, and (3) a Total Direct and Diffuse Radiometer (TDDR) to measure irradiance in seven spectral bands 10 nm wide centered at 0.500, 0.862, 1.064, 1.249, 1.501, 1.651, and 1.750 μm. Identical sets of instruments pointing in the zenith direction were deployed at the surface stations.

The broadband radiometers are described by *Valero et al.* [1982], and the TDDR is described by *Valero et al.* [1989]. A complete description of the calibration of the Radiation Measurement System (RAMS) instruments is given by *Valero et al.* [this issue (a)]. The radiometers were calibrated for power, angular, and spectral response. Power calibrations were made with reference to National Institute of Standards (NIST) primary radiation standard and also with reference to the solar constant using ER-2 high-altitude observations. Angular and spectral response calibrations were made at the laboratory. To verify overall calibrations, all radiometers were compared to each other exposing them simultaneously to clear and cloudy skies radiation fields at the surface. The airborne instruments were also compared in situ by flying the Egrett and Twin Otter aircraft side by side several times during the experiment. From the surface and airborne comparisons we concluded that the radiometric in situ, relative precision of the instruments was about 1%. Generally, the airborne comparisons were made late in the day, at low Sun elevations. The algorithms used for navigational corrections and used to determine the relative Sun-instrument position are described in detail by *Hammer et al.* [1991].

2.3. Instrument Spectral Response Functions

TSBR and FSBR fluxes were reported filtered, that is, convolved with the instrument Spectral Response Function (SRF). No attempt is made to unfilter the observed fluxes for comparison to the model. Instead, the appropriate SRF is applied to the model data before integrating modeled spectral fluxes. Since model spectral resolution exceeds that of the SRFs, a simple binning approach was employed to map the SRFs to the model spectral grid. The SRFs of the airborne and surface RAMS instruments are identical and do not vary in time or space. Approximate squarewave band passes of the TSBR and FSBR are 0.224–3.91 μm and 0.68–3.3 μm, respectively [*Valero et al.*, this issue (a)]. The term "shortwave" will be used to describe modeled and measured fluxes in the TSBR band pass. "Near-infrared" (NIR) refers to the FSBR band pass, and "visible" refers to the TSBR-FSBR difference, that is, the spectral region 0.224–0.68 μm.

2.4. Aircraft Collocation

The flux divergence between the two aircraft has been determined from a subset of the observations when the Egrett was almost directly above the Otter. Radiometric data, when the aircraft were vertically stacked, have been identified using software developed as part of the C4 Integrated Data System (CIDS) (URL = http://www-c4.ucsd.edu/~cids/). The flux divergence has been calculated using measurements separated by less than 0.1 s in time and less than 0.035 degrees (approximately 3.8 km) in latitude and longitude. The flux divergence is relatively insensitive to the spatial separation used to identify stacked aircraft measurements. Constraining the horizontal separation of stacked aircraft to 1 km alters flight average flux divergence by less than 1.5% on October 11 and 30, 1995. The horizontal position of the aircraft has been determined from Global Positioning System (GPS) instruments on both platforms. The pressure altitude derived from measurements of static pressure is used to specify the vertical position of the aircraft. The static pressure is also used to determine the 10 mbar thick model level that corresponds to each flux measurement. Data from the flux radiometers, GPS, and meteorological package on each aircraft are matched pairwise to within the measurement interval of the slower instrument. The approximate sampling rates of the RAMS, GPS, and meteorological parameters are 12, 8, and 0.2 Hz, respectively.

2.5. Time Convention

Henceforth, dates and time of day are presented in YYMMDD and HHMM format. Data for ARESE are archived in

UNIX time (seconds since 700101). To facilitate investigation of diurnal asymmetry, figures showing the diurnal variation of observed quantities are shown in local True Solar Time (TST). By definition, the solar zenith angle θ is minimal at noon TST. The conversion from GMT to TST uses the procedure of *Lenoble* [1993]. TST noon precedes local mean time noon by 13–16 min from 951011–951030. The coordinates of the RAMS instruments at the Cloud and Radiation Testbed (CART) site are 36.6048°N, 97.4841°W. Unless otherwise specified, noontime refers to 1200 TST.

2.6. Narrow Band Model

Spectral fluxes are computed using a standard discrete ordinate radiative transfer code (DISORT) [*Stamnes et al.*, 1988] with 1690 bands from 0.20–5.0 μm. Four streams (two in each hemisphere) are employed. The difference in cloudy sky hemispheric fluxes computed using eight rather than four streams is less than 2 W m^{-2}. The incident solar spectral irradiance is the 1 cm^{-1} resolution modeled solar spectrum of *Kurucz* [1995], normalized to a solar constant of 1367 W m^{-2}. The solar zenith angle is determined using the algorithm of *Michalsky* [1988]. Gaseous absorption of H_2O, CO_2, and O_2 is computed using the Malkmus random band model formulation from 2000 to 17900 cm^{-1} (0.56–5.0 μm) [*Kiehl and Ramanathan*, 1983]. H_2O and O_2 use 10 cm^{-1} band spacing; CO_2 uses 5 cm^{-1}. CO_2 5 cm^{-1} transmissions are evaluated, then averaged to 10 cm^{-1}. Line data for all gases is from the HITRAN96 CDROM [*Rothman et al.*, 1992]. The effective gaseous absorption optical depth of each atmospheric layer is computed from the random band model transmission formula for the direct solar beam across the layer. Thus, in the nonscattering limit, atmospheric absorption equals Malkmus band model absorption. The calculation employs fully monochromatic intervals from 0.20–0.56 μm. O_3 absorption cross sections in the Hartley, Huggins, and Chappuis bands, and O_2 Herzberg continuum absorption are incorporated at 0.02–0.05 μm resolution [*World Meteorological Organization*, 1985]. Atmospheric thermal emission is accounted for; this contributes approximately 0.5 W m^{-2} to the surface insolation in the TSBR band pass at noontime. The model geometry is plane parallel. The effective gaseous optical depths are combined with aerosol and cloud absorption and scattering, allowing detailed calculations of spectral fluxes.

2.7. Water Vapor, Ozone, and Cloud Water

Temperature, pressure, water vapor, ozone, and (on 951030) cloud liquid water path (LWP) are input to the model as time varying atmospheric state parameters. Vaisala sondes measuring pressure, temperature, and water vapor were launched from the CART site every 3 hours. Soundings near 0500, 0800, 1100, 1400, and 1700 TST were linearly interpolated to model time resolution (5–30 min) and logarithmically interpolated to the model vertical grid (10 mbar spacing in the troposphere, 110 levels total). No sonde data are available at the CART site or the boundary facilities at 1700 on 951030, so the 1400 sounding was repeated. H_2O data above the Vaisala sondes are taken from ozonesonde measurements. O_3 profiles are taken from the nearest daily ozonesonde measurement in time. H_2O and O_3 sondes usually ceased operating between 50 and 10 mbar. Standard midlatitude summer data were used to extend the profiles to 1 mbar.

Model LWP on 951030 is from the Pennsylvania State University Microwave Radiometer (MWR) which archived 5 min averages of liquid water. Cloud presence in the model was determined by supersaturation with respect to liquid. Measured total LWP was homogeneously apportioned through the vertical profile of the cloud. All cloud on 951030 is warmer than 0°C and thus modeled as spherical liquid droplets in accordance with Mie theory. A lognormal size distribution is assumed with standard deviation of 1.5 and effective radius r_e = 10 μm. The sensitivity of the model results to other values of r_e is presented in sections 3.1, 3.2, 3.4.3, and 3.5. The optical properties of the droplet distribution were computed from indices of refraction tabulated at a resolution from 0.02 μm in the visible to 0.1 μm in the NIR.

2.8. Aerosol Properties

The model includes radiative effects of a tropospheric mineral dust aerosol and a stratospheric background sulfate aerosol. The sum of the dust and sulfate aerosol extinction is set equal to the diurnally varying extinction optical depth $\tau^{obs}_{0.5\mu}$ measured by the 0.500 μm channel of the Multifilter Rotating Shadowband Radiometer (MFRSR) [*Harrison et al.*, 1994]. The MFRSR is calibrated to a precision of 0.01 optical depths. The measured optical depths are not corrected to eliminate possible biases caused by aerosol forward scattering into the measured beam because this correction factor for the MFRSR looking at a dust aerosol is estimated to be less than 5% (L. Harrison and J. Michalsky, personal communication, 1997).

Indices of refraction for the tropospheric aerosol are taken from the "mineral dust" aerosol of *d'Almeida et al.* [1991]. Size distribution parameters are the ensemble properties of the soil-derived aerosol distributions studied by *Patterson and Gillette* [1977]. The assumed distribution is lognormal, mean radius r_e = 0.4 μm, standard deviation σ = 2.2, and density ρ_{aer} = 2.5 g cm^{-3}. These aerosol properties yield a single scattering albedo ϖ = 0.82 and an asymmetry parameter g = 0.77 at 0.5 μm. The dust aerosol is assumed uniformly mixed in the bottom 100 mbar.

The optical depth of the stratospheric sulphate aerosol over the CART site was estimated from Stratospheric aerosol and gas experiment (SAGE) II data. Both the monthly zonal average data and individual overflights during ARESE suggest a time-invariant stratospheric background aerosol with an extinction optical depth of approximately 0.006 at 0.500 μm was present during ARESE. This optical depth is consistent with independent estimates of the stratospheric aerosol over Laramie, Wyoming (5°N of ARESE), from satellite (SAGE II and halogen occultation experiment (HALOE)) and balloonborne instruments (T. Deshler and M. Hervig, personal communication, 1997). This stratospheric aerosol is assumed to be a sulfuric acid solution which is 75% H_2SO_4 by weight. The H_2SO_4 solution indices of refraction are taken from measurements at 215°K [*Hummel et al.*, 1988]. The assumed H_2SO_4 size distribution is lognormal, mean radius r_e = 0.24 μm, and standard deviation σ = 1.4. These aerosol properties yield a single scattering albedo ϖ = 0.9999999 and an asymmetry parameter g = 0.75 at 0.5 μm. The H_2SO_4 is homogeneously distributed from 10 to 100 mbar.

The simulations below are labeled "clean sky" or "turbid sky," indicating the absence or presence of aerosol in the model, respectively. Turbidity on 951030, when aerosol measurements were unavailable, was set equal to the average value on 951011 (optical depth 0.12 at 0.500 μm) and assumed to be constant throughout the day.

2.9. Surface Albedo

A diurnally symmetric shortwave surface albedo is specified by a curve fit to upward and downward looking surface Solar and Infrared Radiation Observation Station (SIROS) pyranometer observations according to

$$\alpha(\mu) = 0.2\left(\frac{1.6}{1 + 1.2\mu}\right) \quad (1)$$

where $\mu \equiv \cos\theta$ and θ is the solar zenith angle (B. Briegleb, personal communication, 1996). Shortwave albedo is partitioned into visible and NIR components as follows: Using land-surface properties of *Bonan* [1996], the CART site in October is best described as grassy with equal coverage by leaf and stem. Spectral albedos of this surface type are related by $\alpha_{NIR} \approx 2.5\alpha_{vis}$. Observed visible surface insolation is within roughly 15% of NIR surface insolation, so we partition α (1) into equally weighted visible and NIR albedos. The sensitivity of modeled surface insolation to observed diurnal asymmetry in the surface albedo [*Minnis et al.*, 1997] was estimated by computing surface insolation for noontime conditions on 951011 and perturbing the shortwave surface albedo from 0.20 to 0.22, all other parameters held constant. This 10% relative increase in albedo increased surface insolation by only 1.1 W m^{-2}.

2.10. Absorption by O_2-O_2, O_2-N_2, and NO_2

Recent work has shown that the oxygen collision pairs O_2-O_2 and O_2-N_2 absorb a small but significant amount of solar radiation and hence should be considered in attempts to balance the radiation budget [*Pfeilsticker et al.*, 1997; S. Solomon et al., Absorption of solar radiation by water vapor, oxygen, and related collision pairs in the Earth's atmosphere, submitted to *Journal of Geophysical Research*, 1997, hereinafter referred to as Solomon et al., submitted manuscript, 1997]. This study accounts for solar absorption by O_2-O_2, using the absorption spectrum developed by Solomon et al. which includes a 1.26 μm band not considered by *Pfeilsticker et al.* [1997]. Accounting for O_2-O_2 increases clear and overcast sky absorption at noontime by approximately 2 and 2.5 W m^{-2}, respectively. We do not account for the absorption caused by the O_2-N_2 collision complex. For clear sky midlatitude summer conditions at noontime, O_2-N_2 is estimated to absorb 0.2–0.8 W m^{-2} [Solomon et al., submitted manuscript, 1997].

SAGE II overflights during ARESE show the number concentration of NO_2 above 20 km is approximately 2.5×10^{19} m^{-2}. We assumed a free tropospheric NO_2 concentration of 0.15 parts per billion by volume (ppbv) [*Seinfeld*, 1986, p. 37]. This results in a total model column NO_2 burden of 5×10^{19} m^{-2}. This much NO_2 absorbs approximately 0.9 W m^{-2} at noontime in clear skies.

3. Results

The modeling component of this ARESE study quantifies the difference between theory and observations of atmospheric shortwave absorption. As described above, previous studies indicate enhanced absorption (meaning absorption in excess of that predicted by currently accepted theoretical models) occurs in cloudy atmospheres. We show detailed model results from 2 clear sky days and 1 overcast day (951011, 951015, and 951030, respectively). As will be shown below, model bias on the overcast day overwhelms any possible clear sky bias. Thus clear sky results are examined first to better quantify uncertainty in cloudy sky results.

3.1. Observed and Modeled Surface Insolation

Surface insolation $F^{\downarrow}$(sfc) is defined as hemispheric downwelling flux at the surface. Figure 1 shows observed and modeled surface insolation for 951011. Continuous surface RAMS observations exist for 7.1 hours this day. Egrett and Otter aircraft were both aloft for 4.3 hours, and the four overflights of the CART site by the stacked aircraft (henceforth, simply collocations) are indicated by open circles. The fact that 951011 was a clear-sky day can be discerned from the smooth cosine shape of the surface RAMS observations, the Pennsylvania State 94 GHz cloud radar, and the microwave radiometer. High frequency variation in the observed time series is presumably due to water vapor and aerosol variation. Time-mean observed $F^{\downarrow}$(sfc) is 17 W m^{-2} less than the model prediction with the aerosols (dashed curve).

Aerosols consistently reduce the model shortwave bias but not the NIR bias. In the early afternoon the aerosols cause the model to overpredict NIR absorption. At noontime the aerosols (whose total extinction optical depth is roughly 0.12) reduce modeled shortwave and NIR insolation by 25 and 7 W m^{-2}, respectively. Thus the aerosols have a greater effect on visible than NIR insolation. Sensitivity studies to aerosol microphysical properties (e.g., single scattering albedo ϖ and asymmetry factor g) show reasonable assumptions can lead to significant differences in surface insolation. For example, halving the effective radius of the mineral dust aerosol from r_e = 0.4 to 0.2 μm changes ϖ and g from 0.82 and 0.77 at 0.5 μm, respectively, to 0.88 and 0.72. This increases predicted noontime surface insolation by 4 W m^{-2}. On the other hand, a factor of 1.5 increase in the mineral dust loading reduces predicted noontime surface insolation by about 15 W m^{-2}. Without more extensive in situ data on aerosol composition and amount, it is impossible to unambiguously determine which factors significantly contribute to model surface insolation biases.

Model clear sky performance improves on 951015, a pristine clear-sky day shown in Figure 2. Continuous surface observations were made for 8.4 hours this day. Day 951015 was much drier and less turbid than 951011: noontime total precipitable water changed from 20.3 to 11.6 kg m^{-2}, while average aerosol optical depth decreased from 0.12 to 0.04. Unfortunately, both aircraft were grounded on this pristine day. Shortwave surface insolation is very close to the turbid model simulation until about 1400 TST. The time-mean shortwave insolation bias improves from 17 W m^{-2} on 951011 to 11 W m^{-2} on 951015. The time-mean NIR insolation bias is -5 W m^{-2} on both days. The small time-mean NIR bias is partially due to cancellation of biases of opposing signs. Given the 1% accuracy of the radiometers and the large uncertainty in aerosol optical properties, none of these clear-sky biases is considered significant.

Figure 3 shows observed and modeled surface insolation for 951030. Continuous surface RAMS observations exist for 4.0 hours on 951030. Surface insolation, microwave radiometer, cloud radar, and airborne lidar all indicate the CART site was overcast by an unbroken cloud deck for the entire period of RAMS observations. Five aircraft collocations occur over a period of 2.3 hours centered at noontime. H_2O sondes indicate supersaturation (and thus the presence of model cloud) was confined from 600 to 2200 m (910–750 mbar) during midday. The highest frequency forcing in the model simulation is the 5 min average observed LWP from the MWR. This forcing produces the same high frequency variation observed in surface

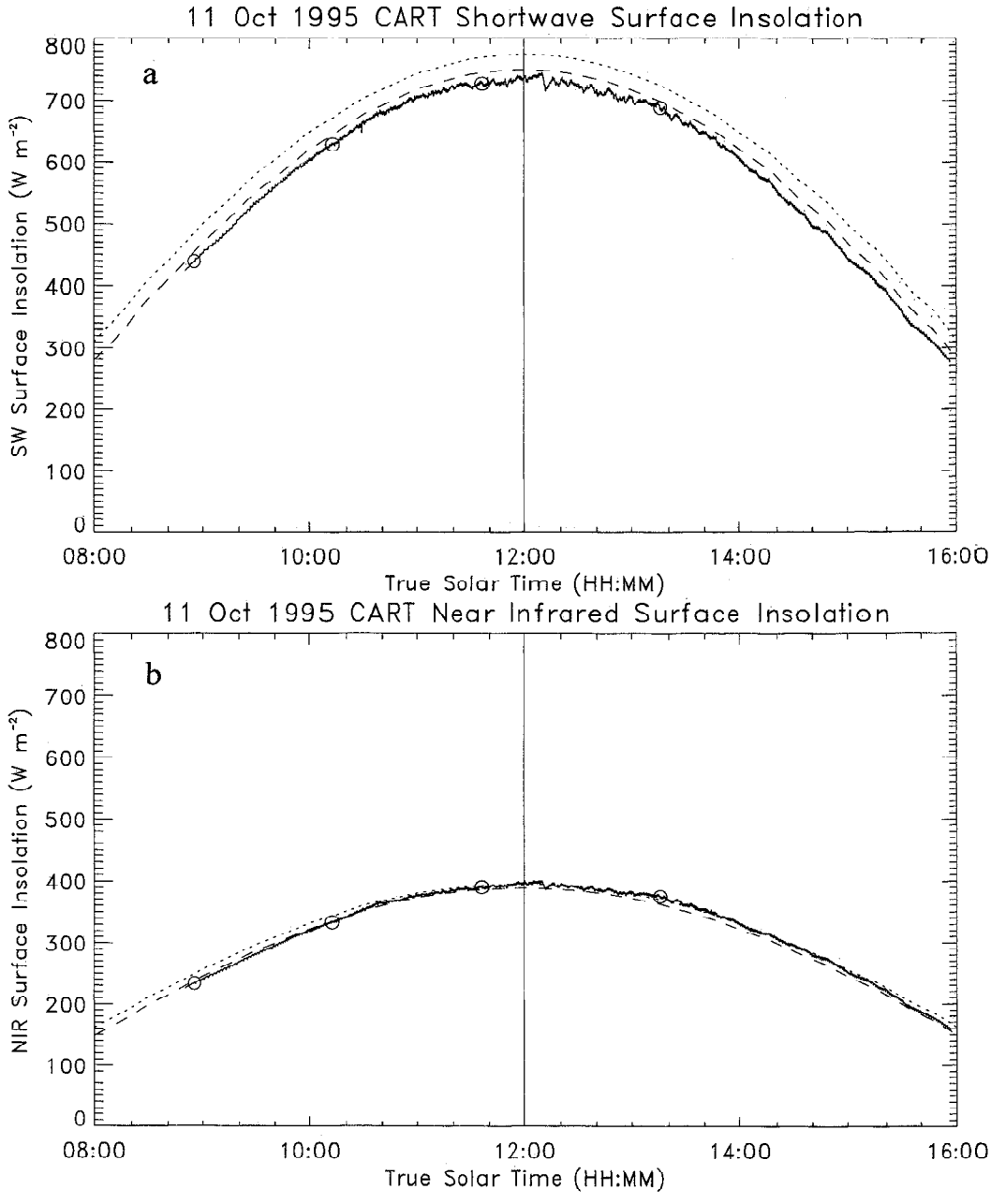

Figure 1. Observed and modeled instantaneous surface insolation at the CART site for 951011. Solid lines show (a) shortwave and (b) NIR observations. Modeled insolation is shown for clean (dotted lines) and turbid (dashed lines) conditions. Model points are located every 15 min about noontime (vertical line). Horizontal tick spacing is 20 min. Open circles represent 3 min averages of collocation events.

insolation, but with a substantial bias. Modeled $F^{\downarrow}$(sfc) exceeds observed by 30–100%, but the locations of extrema are well reproduced. Observed surface insolation falls beneath 30 W m^{-2} about 1325 TST, when the MWR measured LWP in excess of 550 g m^{-2}. Observed and modeled atmospheric transmittance for the five collocation points is discussed in more detail in section 3.4.3 below.

Aerosol forcing varies with the observed insolation because most of the dust aerosol is beneath the cloud deck. The strength of this forcing on 951030 is often comparable to 951011 (Figure 1) because the mineral dust aerosol absorbs strongly in the visible spectrum, where model cloud droplets are weakly absorbing but highly scattering.

Model clear and cloudy sky biases are better understood by viewing Figure 4, which scatterplots observed versus modeled surface insolation for 951011, 951015, and 951030. The number of points in each panel is determined by the time resolution of model simulations for that day (15, 30, and 5 min, respectively) and the period of surface RAMS operation. The model points shown are from turbid sky, not clean sky, simulations. Each panel contains three measures of model performance. RMS error is the root-mean-square of modeled-observed shortwave insolation. The RMS error increases from 14.3 W m^{-2} on 951015 to 67 W m^{-2} on 951030. The magnitudes and causes of the RMS errors are further discussed in terms of the time-mean biases presented in Table 1 below. RMS fit is the root-

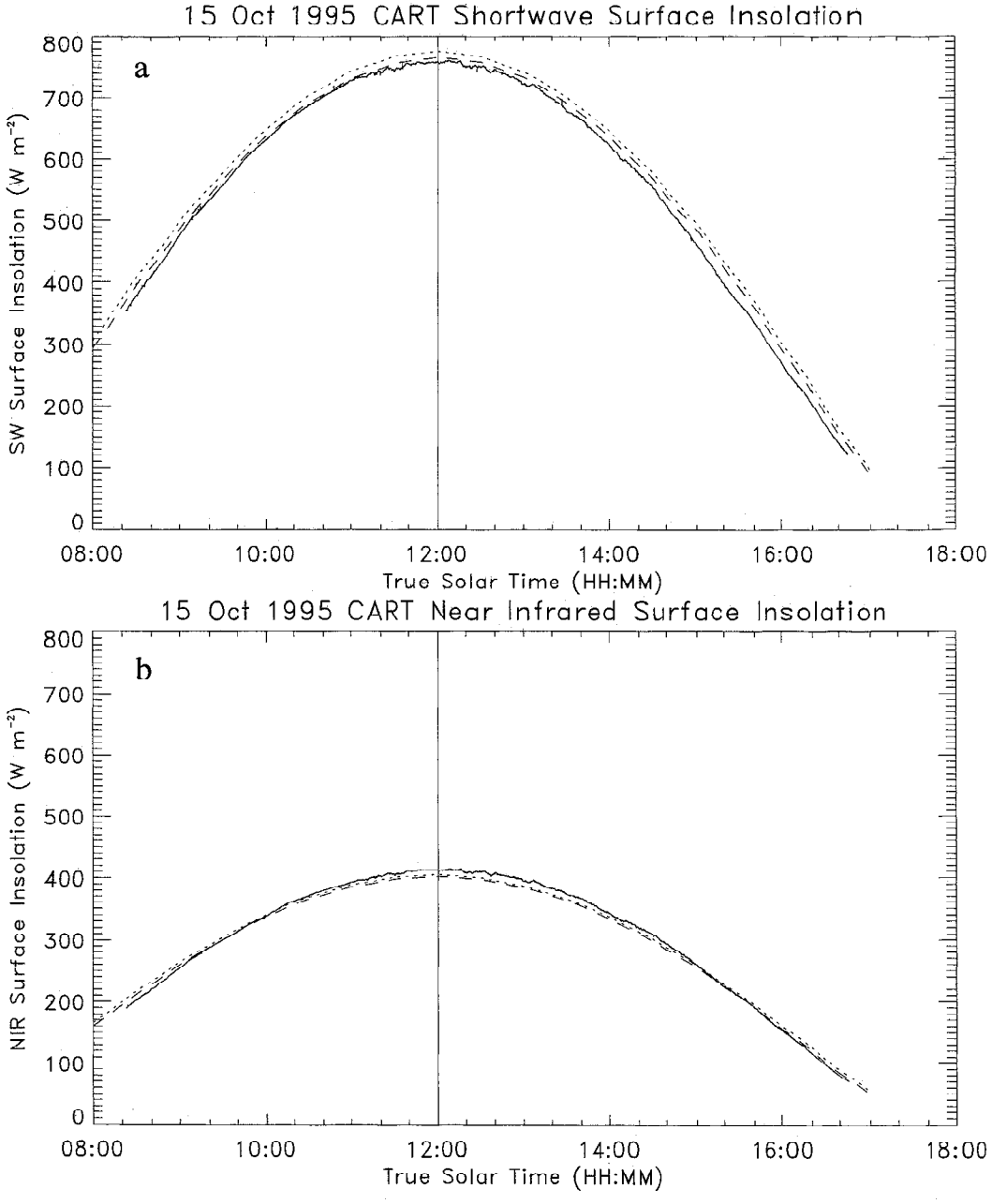

Figure 2. As in Figure 1, but for 951015. Model points are located every 30 min about noontime.

mean-square difference between the model points and the linear least squares regression through the modeled and observed shortwave insolation. The RMS fit of model shortwave insolation to the clear-sky linear regressions is about 4 W m^{-2}, indicating clear-sky model bias is very stable. Model cloudy sky surface insolation bias grows linearly with an RMS scatter of 19 W m^{-2}. Offset is the y intercept of the linear least squares regression. The offsets of the clear-sky shortwave regressions are almost 30 W m^{-2}. These offsets arise from diurnally asymmetric biases, that is, the relatively large biases from 1400 to 1600 TST. The cloudy sky offset, 12 W m^{-2}, is largely due to the diurnal asymmetry of LWP.

Table 1 summarizes observed and modeled time average shortwave $F^{\downarrow}$(sfc) for 951011, 951015, and 951030. The high-resolution model time series used in the averages were generated by linearly interpolating the nearest model simulations in time (5–30 min resolution) to each observed time (~1 s resolution). The model surface insolation biases on 951011 appears to be due to underestimating clear-sky absorption rather than reflection. The improvement of the clear-sky bias on 951015, the drier, more pristine day, is consistent with a model underestimate of aerosol absorption, water vapor absorption, or both. The average cloudy sky model bias is 62 W m^{-2}. The insolation bias is strongly sensitive to assumed cloud droplet effective radius r_e, which we have conservatively set to r_e = 10 μm. A more likely value for the stratus on 951030 is 6–8 μm [e.g., *Heymsfield*, 1993; *Han et al.*, 1994]. Assuming r_e = 7 μm reduces noontime surface insolation by 65 W m^{-2} which eliminates most of the model insolation bias. However, smaller r_e also reduces predicted cloud absorption and increases predicted cloud albedo, in both cases increasing discrepancies between model and observation (sections 3.2 and 3.3). Thus

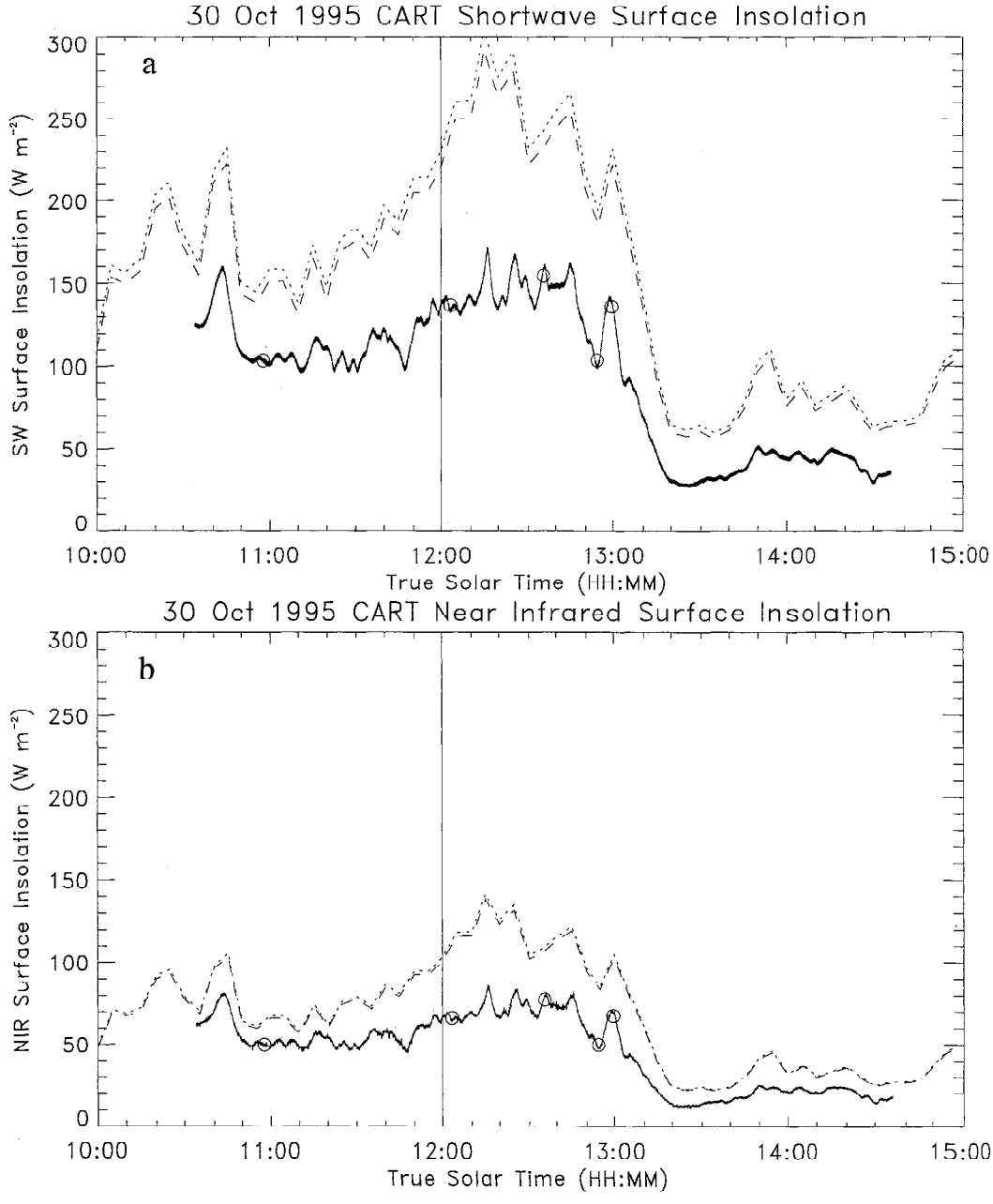

Figure 3. As in Figure 1, but for 951030. Horizontal tick spacing is 10 min. Model points are located every 5 min about noontime.

assuming r_e = 10 μm is conservative because it produces a plausible upper bound for cloud absorption based on our current understanding of cloud physics. This is consistent with our strategy of maximizing modeled atmospheric absorption before confirming or denying the detection of enhanced cloud absorption in ARESE.

As mentioned above, broken cloud did not affect the CART site on 951030. However, the strong horizontal variation in LWP observed by the MWR is also clearly seen in time series of $F^{\downarrow}$(sfc). *Cess et al.* [1996] show time-averaged station data (e.g., surface insolation in Table 1) can be equivalent to spatially averaged data at a fixed time. Flight-averaged data complement instantaneous collocation data by increasing the temporal and spatial dimensions of the sampling. *Valero et al.* [this issue (b), Figure 15] show that averaging the aircraft-measured flux data over the entire duration of the stacked flight (about 80 min) is sufficient to remove temporal sampling errors. These flight-averaged data are helpful in identifying sampling errors in quantities which require aircraft collocation to measure and model (e.g., cloud albedo and absorption) because only five collocation events occurred on 951030. Thus, where informative, we present both collocated and flight-average data below.

Model overestimation of cloudy sky surface insolation has also been reported in independent studies at the CART site [*Charlock and Alberta*, 1996] and at global scales (see discussion by *Cess et al.* [1996]). Overestimating overcast sky surface insolation (i.e., transmission) does not, by itself, constitute evidence of enhanced cloud absorption. However, should the model overpredict reflection while simultaneously overpredict-

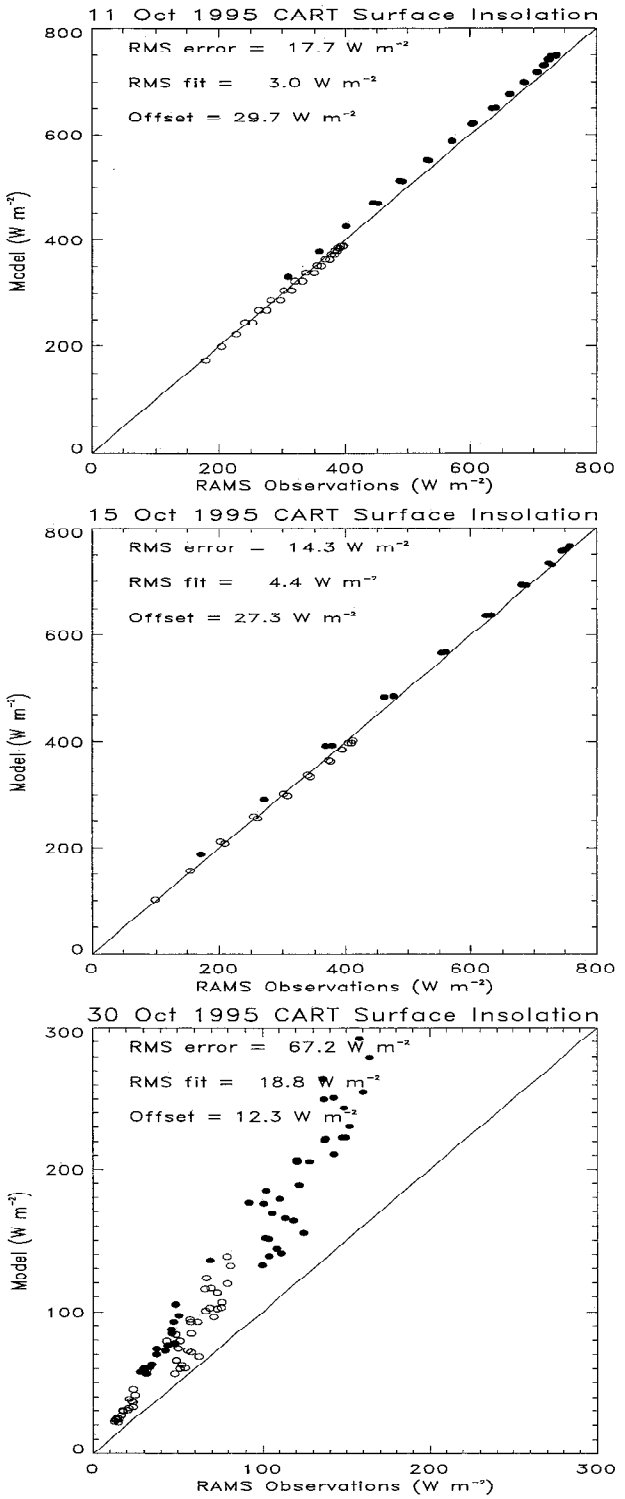

Figure 4. Observed and modeled instantaneous surface insolation at the CART site for 951011, 951015, and 951030. RAMS data are segregated into NIR (open circles) and shortwave (solid circles). Regressions use shortwave data only.

ing transmission, then the model is underestimating absorption. Our study will now show that the model simultaneously overpredicts transmission and reflection, which provides indirect evidence for the detection of enhanced cloud absorption during ARESE.

Table 1. Observed and Modeled Time Average Shortwave $F^{\downarrow}$ (sfc) for 951011, 951015, and 951030

Day	T, hour	Observed, W m^{-2}	Model, W m^{-2}	Bias, W m^{-2}
951011	7.10	597	614	17
951015	8.37	566	577	11
951030	4.04	94	156	62

Averages are computed over the period T of surface RAMS activity. Bias is computed as modeled-observed.

3.2. Observed and Modeled Egrett Albedo

For the purposes of this study, albedo is defined as the ratio of upwelling to downwelling flux at the Egrett flight level, that is, $A \equiv F^{\uparrow}(\text{Egr})/F^{\downarrow}(\text{Egr})$. Figure 5 shows the correlation of modeled and observed Egrett albedo for 951011 and 951030. The model has an absolute clear-sky shortwave albedo bias less than 0.03 during collocation events and less than 0.013 averaged over the flight. Unfortunately, upwelling NIR flux at the Egrett was not recorded on 951011, and no flights occurred on 951015. Modeled NIR albedos from "clear-sky" collocations on partially cloudy days (951013, 951017, and 951019) indicate the absolute clear-sky NIR albedo bias is less than 0.02. However, the possibility of cloud contamination makes clear-sky observations on partially cloudy days tentative at best.

Modeled shortwave albedo exceeds observed albedo on the overcast day, 951030. Observed LWP (used to force the model) and observed and modeled Egrett albedo for 951030 are tabulated in Table 2. The shortwave albedo bias is positive considering either the collocations or the entire flight average. The mean bias is 0.05 during the five collocations and 0.03 over the entire flight. Note the two largest model albedo biases (0.11 and 0.06 for collocations 1 and 4, respectively) coincide with the two largest LWPs. The observed collocated and flight mean NIR albedos (not shown) are 0.45 and 0.47, respectively. The model NIR albedo bias is 0.015 for both collocated and flight averages. The 1% relative precision of the radiometers yields uncertainties in Egrett shortwave albedo of ± 0.01. This uncertainty range, combined with the approximations in the model and its input data, can reconcile collocated modeled-observed albedo disparities smaller than approximately 0.05. However, these model predictions assume $r_e = 10$ μm, a relatively large effective radius for continental stratus. Setting $r_e = 7$ μm increases the model albedo bias by roughly 0.06 over the entire flight.

Model overprediction of overcast sky albedo provides indirect evidence of enhanced cloud absorption for three reasons. First, if observed albedos exceeded modeled, one could argue the LWP of the simulated cloud is too low. On the contrary, the positive albedo bias guarantees, if anything, the simulated cloud is thicker and, due to the assumption of relatively large liquid cloud droplets ($r_e = 10$ μm) for cloud radiative properties, more absorptive than observed. Second, the positive cloud albedo bias implies using the correct (observed) albedo would increase predicted surface insolation. Thus "fixing" the model albedo bias tends to worsen the surface insolation bias shown in section 3.1. Albedo biases of 0.03–0.05 represent 25–40 W m^{-2} of reflected shortwave flux. Combined with the ~60 W m^{-2} insolation bias (Table 1), the model is seen to predict roughly 90 W m^{-2} too much energy in the form of reflected and transmitted flux on the overcast day.

Third, the simultaneous overprediction of Egrett albedo and

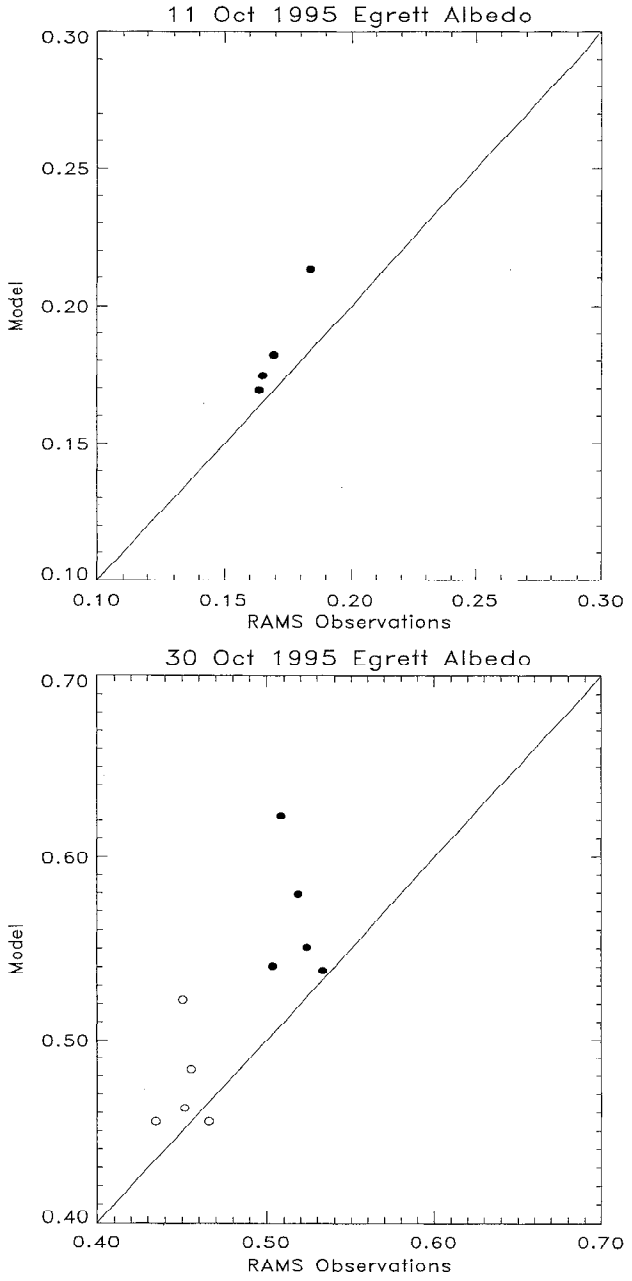

Figure 5. Observed and modeled 3 min averages of collocated Egrett albedo at the CART site for 951011 and 951030. RAMS data are segregated into NIR (open circles) and shortwave (solid circles).

transmission implies that the excess absorption is in the atmosphere (rather than the surface) only if the uncertainty in the surface absorbed flux is small. The agreement between modeled and observed shortwave albedo on 951011 demonstrates that errors in modeled surface albedo (1), and thus surface absorptance, are ≤ 0.03. These small uncertainties in surface albedo can affect only the transmitted fraction (10–20%) of the insolation (~ 800 W m^{-2}) incident on the overcast deck on 951030. Thus surface absorption accounts for less than $0.03 \times 0.20 \times 800 = 5$ W m^{-2} of the inferred excess absorption. The conclusion to draw is that the positive insolation and albedo biases together indicate the model underpredicts atmospheric absorption between the Egrett and the surface.

Table 2. Observed and Modeled Albedo for 951030

	Observation				Model		
t	LWP, g m^{-2}	$F^{\uparrow}$, W m^{-2}	$F^{\downarrow}$, W m^{-2}	A	$F^{\uparrow}$, W m^{-2}	$F^{\downarrow}$, W m^{-2}	A
1	209	413	814	0.51	504	809	0.62
2	117	436	818	0.53	455	846	0.54
3	116	408	810	0.50	450	833	0.54
4	145	423	816	0.52	473	817	0.58
5	128	423	807	0.52	446	811	0.55
1–5 average	143	421	813	0.52	466	823	0.57
Flight average	156	443	813	0.54	478	829	0.58

Shown are observed liquid water path (LWP) (g m^{-2}) and observed and modeled hemispheric fluxes and albedo A at Egrett flight level computed three different ways: times 1–5 show instantaneous A computed from 3 min average fluxes for the five stacked Egrett collocations with the CART site. Following is the average A of these five collocations ("1–5 average"). The final row shows A computed over the entire stacked aircraft flight time ("Flight average"). LWP obtained from the Pennsylvania State University Microwave Radiometer is shown for all cases.

3.3. Direct Observations and Simulations of Atmospheric Absorption

The preceding surface insolation and albedo observations and simulations constitute only indirect evidence of enhanced cloud absorption during ARESE. We now examine stacked aircraft observations and simulations of flux divergence. These data can directly confirm the detection of enhanced cloud absorption [*Valero et al.*, this issue]. The absorption (flux divergence) between the stacked aircraft is obtained by subtracting the net radiative flux at the Otter level from the net flux at the Egrett. Note this absorption is entirely due to processes that occur between the aircraft.

Figure 6 shows observed and modeled atmospheric absorption for 951011. The aircraft were aloft for 4.3 hours this day, but, as mentioned previously, an Egrett NIR radiometer malfunctioned. Therefore only shortwave absorption was measured. The observed and modeled time series show remarkable agreement. The absorption peak at 0930 TST occurs when the Otter drops 100 mbar (1000 m) from its nominal flight level of 830 mbar (1800 m). This increases the absorption path length of water vapor and dust aerosol. Noise in the absorption time series is the sum of the noise from four instruments on two platforms. Upwelling flux seen by the Otter is particularly sensitive to variations caused by the heterogeneous surface albedo beneath.

The model underpredicts absorption by roughly 14 W m^{-2} during each collocation except the first, which it underpredicts by 47 W m^{-2}. The cause of the large negative model bias in the first collocation is not known with certainty, but two independent lines of reasoning suggest this is not a model bias, but a sampling problem. First, Table 3 shows modeled flight average absorption on 951011 is less than observed by only 6.1 W m^{-2}. The fact that the bias during the four collocation events is much reduced in the flight average indicates the average of the collocation points is sensitive to sampling issues on 951011. Second, constraining the horizontal separation of stacked aircraft to 1 km instead of 3.5 km (section 2.4) eliminates the first collocation and halves the collocated average absorption bias from -22 to -11 W m^{-2}.

Figure 7 shows observed and modeled atmospheric absorption for 951030. The high variability of the observations con-

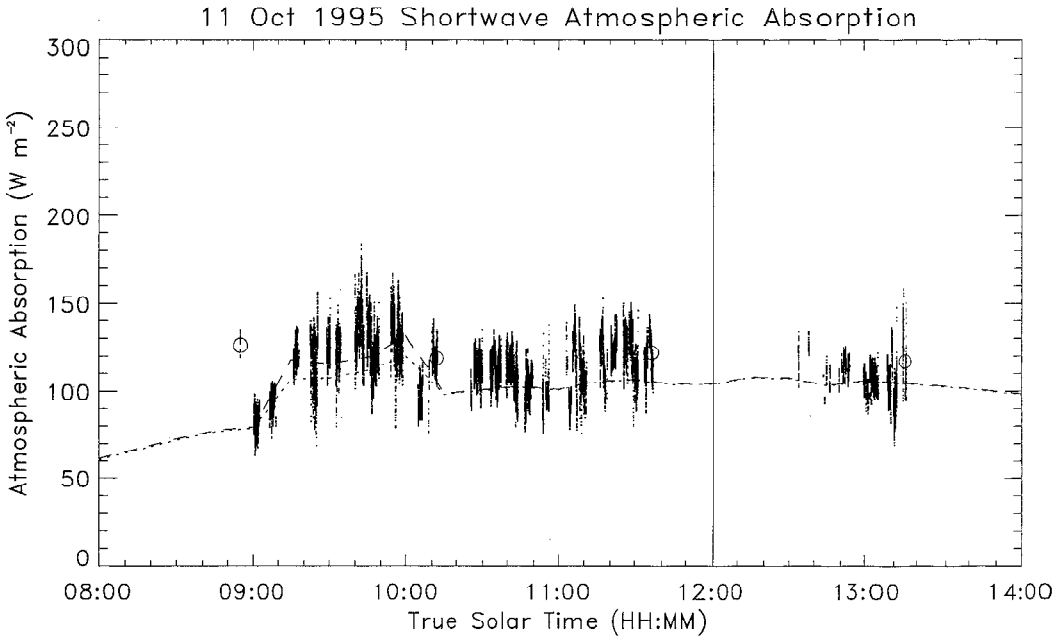

Figure 6. Modeled (at the CART site) and observed instantaneous atmospheric absorption between Egrett and Otter aircraft for 951011. Solid lines show shortwave observations (NIR absorption is not available on 951011 due to instrument malfunction). Modeled absorption is shown for clean (dotted line) and turbid (dashed line) conditions. Horizontal tick spacing is 10 min. Open circles represent 3 min averages of collocation events. Outside Egrett/Otter flight time, model absorption is computed from 165 to 835 mbar.

trast with the smooth model predicted absorption. From 1000 to 1400 TST the effects of strong LWP variation ($80 < \text{LWP} < 540$ g m^{-2}) on modeled atmospheric absorption are barely discernible, although LWP is what forces the good model response in surface insolation (Figure 3). Observed absorption varies over a range of 150 W m^{-2}. Collocated and flight average model absorption both have a substantial negative bias. A strong component of this negative bias is evident in the NIR.

Note the two largest shortwave absorptions observed during collocations (310 and 281 W m^{-2} for collocations 1 and 4, respectively) coincide with the two largest LWPs (Table 2). The observed absorption minima, 58 W m^{-2} at 1237 TST, is probably due to a temporary clearing above the Otter, which was 10 km from the CART site at the time. No instruments at the CART site show any indication of cloud gaps during the aircraft flight on 951030.

The cloudy sky collocated absorption bias is summarized in Figure 8, which shows the correlation of modeled and observed atmospheric absorption on 951030. Again, modeled cloudy sky absorption is nearly constant, while observed cloudy sky (collocated) absorption spans more than 50 W m^{-2}. The large contribution of the NIR to the shortwave cloudy sky absorption bias is clearly seen.

Table 3. Observed and Modeled Clear-Sky Atmospheric Absorption for 951011

t	Observed, W m^{-2}	Model, W m^{-2}	Bias, W m^{-2}
Collocated average	121.2	99.2	−22
Flight average	114.6	108.5	−6.1

The elapsed flight time of the stacked aircraft measurements is 4.32 hours. All four aircraft TSBR instruments were stacked and active for 1.20 hours of the flight. Shown are the observed and modeled average atmospheric absorption computed by averaging the four 3 min averages of collocation events ("Collocated average") and by averaging the entire flight ("Flight average"). Bias is computed as modeled-observed.

A significant component of the cloudy sky absorption bias must, by inference, reside in the visible portion of the spectrum. Here the visible is defined as the TSBR band pass less the FSBR (section 2.3). Table 4 shows observed and modeled shortwave, visible, and NIR absorption between aircraft for 951030. The table shows the direct measurement of enhanced shortwave absorption in cloudy skies and apportions the enhanced absorption into visible and NIR components. Flight observations from four midday hours show the model underpredicts cloudy sky absorption by, on average, 91–111 W m^{-2}. A significant portion of the enhanced absorption occurs at visible wavelengths.

The estimates of excess absorption in Table 4 are the product of a complex combination of models and measurements and contain significant uncertainties. For example, the visible component of enhanced absorption was computed by combining the fluxes measured by eight separate instruments on two different aircraft with simulations of the same eight fluxes. The 1% relative precision in each of the radiometers yields uncertainties in the flight average measurements of shortwave, NIR, and visible flux divergences of ±13, ±7, and ±20 W m^{-2}, respectively. We estimate the uncertainty in the modeled shortwave absorption is ~20 W m^{-2}, mostly due to assumptions regarding the aerosol, cloud droplet distribution, and model geometry. The total (model plus measurement) error in the estimated flight average excess shortwave absorption could be as much as ~35 W m^{-2}, with relatively more error in the visible than the NIR.

Neither direct measurements of cloudy sky absorption (from aircraft) nor indirect measurements (from surface insolation

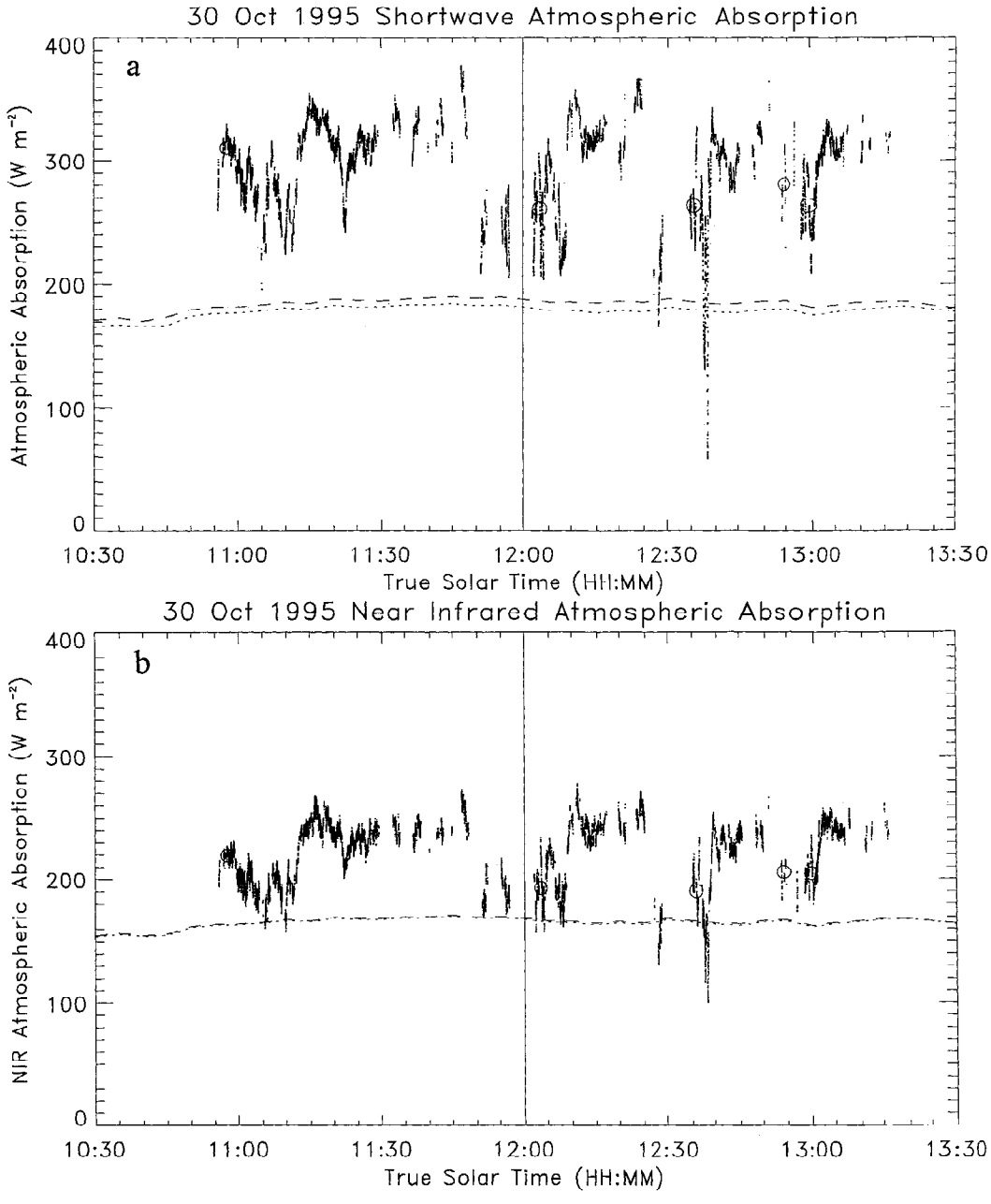

Figure 7. Modeled (at the CART site) and observed instantaneous atmospheric absorption between Egrett and Otter aircraft for 951030. Solid lines show (a) shortwave and (b) NIR observations. Modeled absorption is shown for clean (dotted lines) and turbid (dashed lines) conditions. Open circles represent 3 min averages of collocation events. Outside Egrett/Otter flight time, model absorption is computed from 165 to 935 mbar.

and albedo) agree with the model, which makes conservative assumptions for aerosol amount, cloud thickness, and droplet size. These conservative assumptions add to our confidence that the absorption in the observations is not possible to achieve with any reasonable model assumptions consistent with currently accepted cloud physics.

3.4. Relative Measures of Cloud Absorption

The ARESE Science Plan outlines three additional, independent measures of cloudy sky absorption: shortwave cloud forcing ratio, cloud insolation forcing ratio, and slope of albedo with respect to transmission. These measures are normalized relative to expected clear-sky absorption or insolation. This facilitates intercomparison between geographically and seasonally disparate observations of cloudy sky absorption. These measures further validate direct detection of enhanced cloudy sky absorption by relying on three different sets of independently observed fluxes. Moreover, these strategies extend to instrument configurations besides twin stacked aircraft.

3.4.1. Shortwave cloud forcing ratio. The first strategy combines observations with model results to measure cloudy sky shortwave absorption relative to clear-sky absorption. Shortwave cloud forcing (SWCF) is defined as increase in net shortwave flux at a given level due to cloud scattering and absorption. The model constructs the clear-sky radiation profile by eliminating the radiative effects of all cloud condensate.

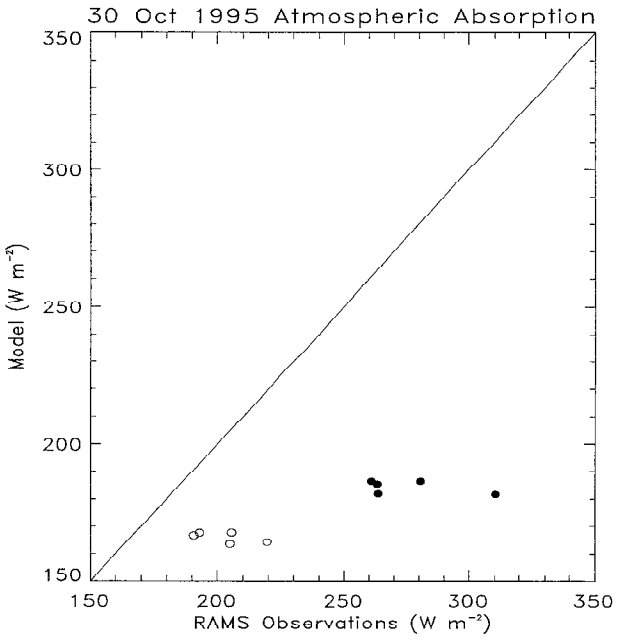

Figure 8. Observed and modeled 3 min averages of collocated atmospheric absorption between Egrett and Otter aircraft at the CART site on 951030. RAMS data are segregated into NIR (open circles) and shortwave (solid circles).

The SWCF ratio R is defined as the ratio of SWCF beneath cloud (Otter level) to SWCF above cloud (Egrett level), that is, $R \equiv$ SWCF(Ott)/SWCF(Egr) [*Pilewskie and Valero*, 1995]. R expresses the cloudy sky atmospheric absorption between the aircraft as a fraction of the clear-sky absorption. An R near unity indicates cloudy sky absorbs as much shortwave radiation as clear sky. Here clear-sky conditions for the cloudy day are determined from the model. Table 5 shows observed and modeled SWCF and R for 951030. The collocated model predictions underestimate R by 18–33%. The average underestimate is 23–25%. Thus observed cloudy sky absorption is in excess of that predicted by currently accepted theoretical models by a significant fraction of clear-sky absorption.

R is sensitive to assumed clear-sky atmospheric turbidity since absorption attributed to the aerosol is not attributed to clouds. Excluding aerosol from the model increases observed R by 0.03–0.04 but increases modeled R by only 0.01–0.02, further biasing the model. Most previous studies defined R as the ratio of surface to Top of Atmosphere (TOA) SWCF. Using this definition, model R decreases by 0.02; observed R should scale similarly.

3.4.2. Cloud insolation forcing ratio. The second strategy for measuring cloudy sky absorption relies on cloud insolation forcing (CIF). CIF is defined as the increase in downwelling flux in cloudy sky relative to clear sky. The CIF ratio C is defined as the ratio of CIF at the surface to SWCF above cloud, that is, $C \equiv$ CIF(sfc)/SWCF(Egr). C, while closely related to R, does not require any instrument to measure upwelling flux beneath clouds. Thus C is not sensitive to assumptions in model surface albedo, a major advantage. C can be measured using one aircraft (or satellite) and an upward looking surface pyranometer.

Collocated observed C ranges from 1.64 to 1.97 on 951030, while model C ranges from 1.31 to 1.34. Collocated and flight average C are shown below in Table 6. The average model bias in collocated C is −0.45, or about 25%. The negative bias in C agrees with the negative bias in R despite the different instruments involved. C is sensitive to model assumptions of aerosol amount and cloud droplet size. Excluding aerosol from the model increases observed C by 0.06 but modeled C by only 0.04, further biasing the model. Most previous studies defined C as the ratio of surface CIF to TOA SWCF. Using this definition, model C increases by 0.02; observed C should scale similarly.

3.4.3. Slope of albedo versus transmission. The final strategy for measuring cloudy sky absorption uses observed transmission and albedo to determine C. It is easy to show $C = -\Delta T/\Delta A$, where T and A are transmission (Egrett to surface) and albedo (Egrett level), respectively, and Δ denotes the all sky minus clear-sky difference. This method of measuring the CIF ratio requires no model data if $\Delta T/\Delta A$ is evaluated by a linear regression (from multiple observations), a major advantage. For convenience, we define β as the magnitude of the slope of the linear regression; that is, $\beta = |\Delta A/\Delta T|$. Thus β^{-1} is an independent estimate of C requiring no model data.

Figure 9 plots observed and modeled transmission against Egrett albedo. All 22 collocations which occurred on 951011, 951013, 951017, 951019, and 951030 are represented by solid circles. As already mentioned, 951011 and 951030 are completely clear and overcast days at the CART site; these days are without broken cloud effects. 951013, 951017, and 951019 were all partially cloudy days. These 3 days have been introduced to improve the statistics and provide data for the intermediate range between clear sky ($T \sim 0.8$) and thick overcast ($T \sim 0.2$). The nine collocations from 951017 and 951019 occurred during clear zenith conditions, but surrounding broken cloud often enhanced T. The model values for these 2 days represent perfectly clear conditions and cluster near $T \sim 0.75$. The four collocations on 951013, which was mostly cloudy, span the range $0.2 \lesssim T \lesssim 0.8$. No attempt was made to model 951013, but the observed values are included. The slope β of the least squares fit to the observed data is 0.58.

The model β is sensitive to cloud droplet size. Choosing $r_e = 7$ μm (open triangles) better reproduces observed midday transmission (at the expense of reducing model absorption), as

Table 4. Observed and Modeled Shortwave, Visible, and NIR Absorption Between Aircraft for 951030

	Observation			Model			Difference		
t	SW, W m^{-2}	Visible, %	NIR, %	SW, W m^{-2}	Visible, %	NIR, %	SW, W m^{-2}	Visible, %	NIR, %
Collocated average	276	26	74	184	10	90	91	60	40
Flight average	296	25	75	185	10	90	111	51	49

Shown are shortwave absorption (W m^{-2}) and its percent partitioning into visible and NIR components.

Table 5. Observed and Modeled SWCF and R for 951030

	Observation			Model		
t	SWCF (Egr), W m^{-2}	SWCF (Ott), W m^{-2}	R	SWCF (Egr), W m^{-2}	SWCF (Ott), W m^{-2}	R
1	−256	−421	1.65	−351	−387	1.10
2	−309	−420	1.36	−299	−336	1.12
3	−276	−389	1.41	−295	−330	1.12
4	−269	−404	1.50	−319	−359	1.13
5	−274	−393	1.43	−294	−331	1.13
1–5 average	−277	−405	1.46	−312	−349	1.12
Flight average	−303	−452	1.49	−322	−360	1.12

Shown is SWCF at flight level computed three different ways: times 1–5 show instantaneous SWCF computed from 3 min averages of net fluxes for the five stacked aircraft collocations with the CART site. Following is the average SWCF of these five collocations ("1–5 average"). Last is SWCF computed over the entire stacked aircraft flight ("Flight average"). R, the ratio of Otter to Egrett SWCF, is shown for all cases.

mentioned in section 3.1. The smaller droplets reduce T and enhance A by the same proportion, which steepens the linear regression. Using $r_e = 7$ μm instead of 10 μm in the regression causes model β to increase from 0.71 to 0.73. This is another example of model inability to simultaneously and accurately predict two members of the set transmission, reflection, and absorption.

3.5. Summary of Relative Measures

The results of the three independent strategies for measuring relative cloudy sky absorption are summarized in Table 6. R, C, and modeled β depend on model data and are therefore sensitive to model assumptions. Thus our best estimates of R, C, and β are given as ranges. The ranges given for these parameters measure uncertainty due to choice of cloud droplet effective radius and aerosol amount. Lower and upper bounds for R and C are obtained by including and excluding the aerosol extinction measured by the MFRSR. The effects of different aerosol assumptions on R and C can be estimated using the range provided by these no aerosol and best guess aerosol cases. Lower and upper bounds for modeled β are obtained by specifying a cloud droplet effective radius r_e of 7 and 10 μm, respectively.

4. Discussion and Summary

The results of section 3 can be summarized separately in terms of clear-sky conditions and cloudy conditions. For clear-sky conditions there is good agreement between observed and modeled radiative properties, given the limited knowledge of aerosol properties. There is a distinct indication that on 951011 the aerosol optical depth has been underestimated. This underestimation could be due to poor characterization of aerosol optical properties due to limited observations. The optical properties used in the present study rely heavily on assumptions about the physical and chemical nature of the aerosol (i.e., size distribution, refractive index, shape, etc.). Improved in situ observations of these aerosol properties would greatly improve any attempt at explaining the remaining biases in radiative fluxes. It is also important to emphasize that aerosols at the SGP are very important for explaining the radiative budget of this region. For October 11 the presence of aerosols alters the shortwave surface insolation by roughly 30 W m^{-2}. The improved agreement on the relatively pristine day, 951015, between observed and modeled radiative fluxes supports the conclusion that there is no evidence for enhanced clear-sky absorption during ARESE. These findings support the results of recent studies of W. C. Conant et al. (Solar absorption and atmospheric water vapor: Current status of model-observation comparisons, submitted to *Tellus*, 1997) and *Vogelmann et al.* [1997].

The results for the cloud-covered day, 951030, are in stark contrast to the clear-sky days. For this day there is a distinct bias between observed and modeled radiative fluxes. Note that the present study employed an effective drop size of 10 μm. This is a very conservative estimate of drop size for continental conditions. Typical effective drop sizes for midcontinental regions are more like 6–7 μm. Sensitivity studies with an effective drop size of 7 μm lead to a larger bias in cloud absorption between observations and the model. Note that all supporting observations indicate no breaks in the clouds over the Central Facility. Also, *Valero et al.* [this issue (b)] find no indication of photon leakage from the sides of clouds on 951030. Thus there is significantly more shortwave absorption within clouds compared to model predictions. It is also important to note that a significant portion of this enhanced absorption occurs in the visible part of the spectrum. The presence of shortwave ab-

Table 6. Summary of Three Independent, Relative Measures of Cloudy Sky Absorption

	Observation			Model		
	R	C	β	R	C	β
Collocated average	1.46–1.50	1.79–1.85	0.58	1.12–1.14	1.34–1.37	0.71–0.73
Flight average	1.49–1.52	1.66–1.72		1.12–1.13	1.33–1.37	

Shown are the range of shortwave cloud forcing ratio $R \equiv$ SWCF(Ott)/SWCF(Egr), cloud insolation forcing ratio $C \equiv$ CIF(sfc)/SWCF(Egr), and albedo-transmission slope $\beta \equiv |\Delta A/\Delta T|$. All quantities are computed from time average fluxes.

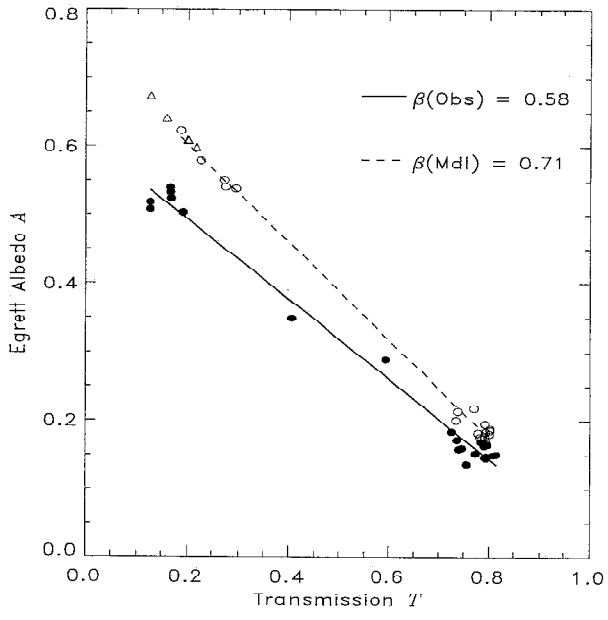

Figure 9. Observed transmission (Egrett to surface) is plotted against Egrett albedo for all collocation events occurring on 951011, 951013, 951017, 951019, and 951030. Observations (solid circles) are computed from 3 min average fluxes collocated with the CART site. Cloudy sky model simulations for 10 and 7 μm cloud droplet effective radius are shown with open circles and triangles, respectively. Model values from 951013 are excluded. Linear regression and slope magnitude (β) are shown for observations (solid line) and for r_e = 10 μm model simulations (dashed line).

sorption in the visible part of the spectrum raises questions concerning any earlier model studies which implicitly assume no absorption in this part of the spectrum.

One of the goals of the ARESE science plan was to employ the same analysis methods used by *Cess et al.* [1995], *Ramanathan et al.* [1995], and *Pilewskie and Valero* [1995] to see if similar conclusions result over the SGP site. The results in Table 6 indicate that the ratio of cloud forcing from observations is approximately 1.5 compared to the model ratio of 1.1. Cess et al. obtained a ratio of 1.41 for the Boulder tower data and a value of 1.1 from the NCAR community climate model (CCM2) simulations for that region. Ramanathan et al. and Pilewskie and Valero found an R value of approximately 1.5 for the warm pool region. Thus the ARESE data analysis in terms of R supports the previous three studies. In terms of the slope of the relation between albedo and transmission, Cess et al. found slopes in the range of 0.52–0.60, while the general circulation model (GCM) slopes ranged from 0.7 to 0.9. Pilewskie and Valero measured slopes from 0.48 to 0.61. The results in Table 6 indicate a slope of 0.58 from the observations, while the computed slopes ranged from 0.71 to 0.73. Thus the results for the slope analysis from ARESE support the results of Cess et al. and Pilewskie and Valero. In terms of the cloud insolation forcing ratio, Cess et al. [1996] found a value of 1.68 for the Boulder tower region from their observations and a value of 1.25 from a GCM. Again, the results from ARESE of 1.66–1.72 are in good agreement with the Cess et al. results, while the model results of 1.33–1.37 are close to what Cess et al. found. Thus the findings of this study are in excellent agreement with the previous studies by *Cess et al.* [1995, 1996], *Ramanathan et al.* [1995], and *Pilewskie and Valero* [1995]. This comparison supports both the analysis methods and conclusions reached by these four studies. The conclusions of the present study complement and support the results of *Valero et al.* [this issue (b)] which focused on a number of cloudy sky days during ARESE.

In conclusion, this study finds, within the uncertainty of assumed aerosol properties, no evidence for enhanced absorption in the clear-sky during ARESE, but strong evidence for the presence of enhanced absorption in the cloudy sky. The ultimate cause(s) for this absorption, both in the visible and near-infrared parts of the spectrum, is (are) unknown. Further information on the spectral distribution of shortwave cloud absorption should help determine the causal mechanism.

Acknowledgments. The authors thank S. Carson for processing sonde data. B. Briegleb developed the surface albedo parameterization (1) and assisted model development. Discussions with R. Cess, V. Ramanathan, M.-H. Zhang, and comments from two anonymous reviewers improved the presentation of this study. Discussions with S. Solomon and R. Portmann allowed us to estimate the absorption of O_2-O_2 and O_2-N_2. T. Deshler and M. Hervig provided helpful analyses of the stratospheric aerosol characteristics during ARESE. Thanks to J. Michalsky for contributing the MFRSR data and solar ephemeris routines. SAGE II aerosol extinction and NO_2 data were obtained from the NASA Langley Research Center EOSDIS Distributed Active Archive Center. This research was supported in part by DOE ARM Program grants DEFG0593ER61376 (JTK and CSZ), DEFG0391ER61198 (WDC), and DEFG0395ER61983 (FPJV). WDC was additionally supported by grant NSF ATM94-05024 to the Center for Clouds, Chemistry, and Climate (C4). The authors gratefully acknowledge the many contributions that made ARESE possible. ARESE was conducted under the auspices of the Department of Energy's Atmospheric Radiation Measurement (ARM) Program and its Unmanned Aerospace Vehicle (ARM-UAV) component, with funding provided through DOE's ARM program and DOD's Strategic Environmental Research and Development Program (SERDP). The NASA Radiation Sciences Program facilitated the use of the ER-2 aircraft during ARESE. Numerous discussions amongst the ARESE, ARM, and ARM-UAV Science Teams helped shape the experiment and its subsequent analysis. A dedicated, multilaboratory field team spent more than 6 weeks in the field conducting the experiments on which this analysis is based. Without all these, ARESE would not have been possible.

References

Arking, A., Absorption of solar energy in the atmosphere: Discrepancy between model and observations, *Science*, *273*, 779–782, 1996.

Bonan, G. B., A land surface model (LSM version 1.0) for ecological, hydrological, and atmospheric studies: Technical description and user's guide, *NCAR Tech. Rep. TN-417+STR*, Natl. Cent. for Atmos. Res., Boulder, Colo., 1996.

Cess, R. D., et al., Absorption of solar radiation by clouds: Observations versus models, *Science*, *267*, 496–499, 1995.

Cess, R. D., M. H. Zhang, X. Jing, and V. Dvortsov, Absorption of solar radiation by clouds: Interpretations of satellite, surface, and aircraft measurements, *J. Geophys. Res.*, *101*(D18), 23,299–23,309, 1996.

Charlock, T. P., and T. L. Alberta, The CERES/ARM/GEWEX experiment (CAGEX) for the retrieval of radiative fluxes with satellite data, *Bull. Am. Meteorol. Soc.*, *77*(11), 2673–2683, 1996.

d'Almeida, G. A., P. Koepke, and E. P. Shettle, *Atmospheric Aerosols: Global Climatology and Radiative Characteristics*, A. Deepak, Hampton, Va., 1991.

Hammer, P. D., F. P. J. Valero, and S. Kinne, The 27–28 October 1986 FIRE cirrus case study: Retrieval of cloud particle sizes and optical depths from comparative analyses of aircraft and satellite-based infrared measurements, *Mon. Weather Rev.*, *119*(7), 1673–1692, 1991.

Han, Q., W. B. Rossow, and A. A. Lacis, Near-global survey of effec-

tive droplet radii in liquid water clouds using ISCCP data, *J. Clim.*, *7*(4), 465–497, 1994.

Harrison, L., J. Michalsky, and J. Berndt, Automated multifilter rotating shadow-band radiometer: An instrument for optical depth and radiation measurements, *Appl. Opt.*, *33*(22), 5118–5125, 1994.

Heymsfield, A. J., Microphysical structures of stratiform and cirrus clouds, in *Aerosol-Cloud-Climate Interactions*, edited by P. V. Hobbs, chap. 4, pp. 97–121, Academic, San Diego, Calif., 1993.

Hummel, J. R., E. P. Shettle, and D. R. Longtin, A new background stratospheric aerosol model for use in atmospheric radiation models, *Tech. Rep. AFGL-TR-88-0166*, Air Force Geophys. Lab., Hanscom Air Force Base, Mass., 1988.

Kiehl, J. T., and V. Ramanathan, CO_2 radiative parameterization used in climate models: Comparison with narrow band models and with laboratory data, *J. Geophys. Res.*, *88*(C9), 5191–5202, 1983.

Kiehl, J. T., and K. E. Trenberth, Earth's annual global mean energy budget, *Bull. Am. Meteorol. Soc.*, *78*(2), 197–208, 1997.

Kurucz, R. L., The solar irradiance by computation, in *Proceedings of the 17th Annual Review Conference on Atmospheric Transmission Models*, vol. 274, p. 332, Philips Lab., Geophys. Dir., Hanscom AFB, Mass., 1995.

Lenoble, J., *Atmospheric Radiative Transfer*, A. Deepak, Hampton, Va., 1993.

Michalsky, J. J., *The Astronomical Almanac*'s algorithm for approximate solar position (1950–2050), *Sol. Energy*, *40*(3), 227–235, 1988.

Minnis, P., S. Mayor, W. L. Smith Jr., and D. F. Young, Asymmetry in the diurnal variation of surface albedo, *IEEE Trans. Geosci. Remote Sens.*, *35*, 879–891, 1997.

Patterson, E. M., and D. A. Gillette, Commonalities in measured size distributions for aerosols having a soil-derived component, *J. Geophys. Res.*, *82*(15), 2074–2082, 1977.

Pfeilsticker, K., F. Erle, and U. Platt, Absorption of solar radiation by atmospheric O_4, *J. Atmos. Sci.*, *54*(7), 933–939, 1997.

Pilewskie, P., and F. P. J. Valero, Direct observations of excess solar absorption by clouds, *Science*, *267*, 1626–1629, 1995.

Ramanathan, V., B. Subasilar, G. J. Zhang, W. Conant, R. D. Cess, J. T. Kiehl, H. Grassl, and L. Shi, Warm pool heat budget and shortwave cloud forcing: A missing physics?, *Science*, *267*, 499–503, 1995.

Rothman, L. S., et al., The HITRAN molecular database: Editions of 1991 and 1992, *J. Quant. Spectrosc. Radiat. Transfer*, *48*(5/6), 469–507, 1992.

Seinfeld, J. H., *Atmospheric Chemistry and Physics of Air Pollution*, John Wiley, New York, 1986.

Stamnes, K., S. C. Tsay, W. Wiscombe, and K. Jayaweera, Numerically stable algorithm for discrete-ordinate-method radiative transfer in multiple scattering and emitting layered media, *Appl. Opt.*, *27*(12), 2502–2509, 1988.

Stephens, G. L., and S.-C. Tsay, On the cloud absorption anomaly, *Q. J. R. Meteorol. Soc.*, *116*, 671–704, 1990.

Valero, F. P. J., W. J. Y. Gore, and P. M. Giver, Radiative flux measurements in the troposphere, *Appl. Opt.*, *21*(5), 831–838, 1982.

Valero, F. P. J., T. P. Ackerman, and W. J. Y. Gore, The effects of the Arctic haze as determined from airborne radiometric measurements during AGASP II, *J. Atmos. Chem.*, *9*, 225–244, 1989.

Valero, F. P. J., A. Bucholtz, B. C. Bush, S. K. Pope, W. D. Collins, P. Flatau, A. Strawa, and W. J. Y. Gore, The Atmospheric Radiation Measurement Enhanced Shortwave Experiment (ARESE): Experimental and data details, *J. Geophys. Res.*, this issue (a).

Valero, F. P. J., R. D. Cess, M. Zhang, S. K. Pope, A. Bucholtz, B. Bush, and J. Vitko Jr., Absorption of solar radiation by the cloudy atmosphere: Interpretations of collocated aircraft measurements, *J. Geophys. Res.*, this issue (b).

Vogelmann, A. M., V. Ramanathan, W. C. Conant, and W. E. Hunter, Observational constraints on the non-lorentzian continuum effects in the near-infrared solar spectrum using ARM ARESE data, *J. Quant. Spectrosc. Radiat. Transfer*, in press, 1997.

Waliser, D. E., W. D. Collins, and S. P. Anderson, An estimate of the surface shortwave cloud forcing over the western Pacific during TOGA COARE, *Geophys. Res. Lett.*, *23*, 519–522, 1996.

World Meteorological Organization, Atmospheric ozone 1985, *Tech. Rep. 16*, Global Ozone Res. and Monit. Proj., Geneva, 1985.

W. D. Collins, J. T. Kiehl, and C. S. Zender, National Center for Atmospheric Research, P.O. Box 3000, Boulder, CO 80307. (e-mail: wcollins@ncar.ucar.edu; jtkon@ncar.ucar.edu; zender@ncar.ucar.edu)

A. Bucholtz, B. Bush, S. K. Pope, and F. P. J. Valero, Scripps Institution of Oceanography, University of California at San Diego, La Jolla, CA 92092. (e-mail: anthony@arlo.ucsd.edu; bbush@arlo.ucsd.edu; pope@arlo.ucsd.edu; fvalero@ucsd.edu)

J. Vitko, Jr., Sandia National Laboratories, POB 969, MS 9056, Livermore, CA 94551-0969. (e-mail: jvitko@sandia.gov)

(Received January 24, 1997; revised June 12, 1997; accepted June 16, 1997.)